New insights into the role of *Cutibacterium acnes*-derived extracellular vesicles in inflammatory skin disorders

Maria Pol Cros[(1)] , Júlia Mir-Pedrol[(1)(2)], Lorena Toloza[(1)], Nastassia Knödlseder[(1)], Marc Güell[(1)], Julien Maruotti[(3)], Christos C. Zouboulis[(4)] and Maria-José Fábrega Fernández[(1)*].

[(1)] Department of Medicine and Life Sciences, Universitat Pompeu Fabra, Barcelona, ES

[(2)] Universitaet Tuebingen Fachbibliothek Mathematik und Physik Tubingen, Baden-Württemberg, DE.

[(3)] Phenocell, Grasse, FR.

[(4)] Hochschulklinik für Dermatologie, Venerologie und Allergologie, Immunologisches Zentrum. Städtisches Klinikum Dessau. Medizinische Hochschule Brandenburg Theodor Fontane und Fakaltät für Gesundheitswissenschaften Brandenburg. Auenweg.

* maria-jose.fabrega@upf.edu

ABSTRACT

Background: *Cutibacterium acnes* (*C. acnes*) is one of the most prevalent bacteria that form the human skin microbiota and, depending on multifactorial conditions it can help to maintain the skin homeostasis. Actually, different phylotypes of *C. acnes* have been associated with different degrees of acne vulgaris development, while others, such as the H1 subtype, have been detected in patients with non-acneic skin. However, due to the physiology of the skin, the skin microbiota neither has direct access to the skin's sebaceous glands nor to the main immune cells, as they are protected by a sebum layer. Therefore, the inter-kingdom communication relies on secreted factors and bacterial extracellular vesicles (EVs). In this context, the purpose of this project was to study the role of EVs secreted by three different phylotypes of *C. acnes* (A1 as pathogenic, H1 as beneficial and H2 as commensal).

Results: Main findings showed that the proteomic profile of the cargo embodied in the EVs reflects unique characteristics of the different *C. acnes* phylotypes in terms of lifestyle, survival and virulence. Moreover, *in vitro* skin models showed an extended pro-inflammatory modulation of A1 EVs, while H1 EVs displayed a high sebum-reducing potential.

Conclusions: This study has highlighted the role of *C. acnes* EVs as key modulators during skin alterations, specially H1 EVs as an alternative based-natural treatment to fight acne vulgaris symptomatology.

Keywords: Microbiome, Extracellular vesicles (EVs), *Cutibacterium acnes*, Skin inflammation and Acne vulgaris.

1. INTRODUCTION

The human body harbours a flourishing diversity of microbes that form a dynamic and functional system that develops in synergy with the physiological development of its host (Rackaityte & Lynch, 2020). The human microbiome resides primarily in the skin, the oral mucosa and the gastrointestinal tracts (Paetzold et al., 2019). Recent data demonstrates that the specific composition of the microbial community is associated with health and disease, which suggests that a detailed characterization of the microbial community would reveal important commensal host-microbiome as well as microbe-microbe interactions with therapeutic implications (Blum, 2017). Over the past decade, researchers have discovered evidence of extensive communication between bacteria, skin cells and immune cells. These interactions are aimed at strengthening and repairing the barrier formed by the skin, reinforcing the body's defences against infection and reducing excess inflammation (Eisenstein, 2020). Nonetheless, failure of this communication can disrupt the protective barrier of the skin and lead to dysbiosis between commensals and pathogens.

One of the most common bacteria present in the normal human skin microbiota is the Gram-positive anaerobic bacterium, *Cutibacterium acnes* (*C. acnes*) which dominates the upper 1.9mm

51 of terminal of pilosebaceous units (Jahns & Alexeyev, 2014; McLaughlin et al., 2019). *C. acnes*
52 helps to preserve and support the natural microbial balance of the skin but under certain
53 conditions, it can also substantially alter its local environment and cause disease (Christensen et
54 al., 2016; O'Neill & Gallo, 2018; Shu et al., 2013). In fact, this bacterium is linked to a wide
55 range of skin diseases, including acne vulgaris. Although the aetiology and pathogenesis of acne
56 are still uncertain, microbiome alterations are thought to be one of the principal mechanisms
57 behind the development of acne (Paetzold et al., 2019). Recently, some authors have described
58 that different phylotypes of *C. acnes* have different degrees of association with acne vulgaris
59 (Fitz-Gibbon et al., 2013; Lomholt & Kilian, 2010; McDowell et al., 2013; McLaughlin et al.,
60 2019). This brings into question how bacteria communicate with host cells to maintain
61 homeostasis of the skin microbiota if sebaceous glands and immune cells are protected by a layer
62 of sebum from external environment and skin microorganisms. This communication is known to
63 be mediated by bacterial extracellular vesicles (EVs), which are nano-sized lipid bilayer vesicles
64 approximately 20-500 nm in diameter that can pass through the lipid barrier and interact with host
65 cells (Bajic et al., 2020; Brown et al., 2015).
66 Since EVs play a key role in interkingdom communication and immune modulation, in the present
67 study, different *in vitro* models mimicking human skin have been established to assay the
68 potential of different *C. acnes* EVs. In this context and based on previous publications (Choi et
69 al., 2018a; Chudzik et al., 2022; Paetzold et al., 2019), we decided to study the role that EVs from
70 three different phylotypes of *C. acnes* play in the onset of acne, considering *C. acnes* A1
71 phylotype (clade IA1) as a pathogenic phylotype, *C. acnes* H1 phylotype (clade IB) as a probiotic
72 phylotype, and *C. acnes* H2 phylotype (clade IB) as a commensal one. Moreover, proteomic
73 characterization of *C. acnes* A1, H1 and H2 EVs has been carried out to determine the relationship
74 of their protein cargo with the skin microbiota. Finally, a novel model mimicking acne-prone skin
75 has been set up in which the sebum-reducing potential of EVs from different *C. acnes* phylotypes
76 has also been tested.
77
78 **2. MATERIALS AND METHODS**

79 **2.1 Bacterial phylotypes and culture conditions**

80 *C. acnes* phylotypes used in this study were extracted from healthy human skin (A1 and H1) or
81 commercially acquired (H2, KPA17202 from DSMZ), typed by SLST typing and we previously
82 sequenced. Sequencing data can be found in the European nucleotide Archive under project
83 number PRJEB42527.

84 Initial cultures were always started from glycerol stocks (stored at −80°C) and seeded on Brucella
85 agar plates which were incubated for 4-5 days at 37°C under anaerobic conditions using the BD
86 GasPak EZ anaerobic bag system.

87 **2.2 Isolation of EVs**

88 The process followed for the isolation of EVs consisted of several steps: cultivation,
89 centrifugation, concentration or ultrafiltration and ultracentrifugation (Fig. S1).

90 In the cultivation step, *C. acnes* phylotypes A1, H1 and H2 were collected from a Brucella agar
91 plate using sterile swabs (Deltalab) and were transferred into 1 L of Brucella liquid medium. After
92 7 to 10 days at 37°C with 300 rpm of stirring and maintaining anaerobic conditions, the culture
93 was centrifuged in 250 mL sterile bottles at 10,000 x g for 30 min and at 4°C. For this step, a
94 Beckman Coulter Avanti JXN-26 high-velocity centrifuge with the J-LITE JLA-16.250 Fixed-
95 Angle Aluminium Rotor were used. Then, the pellet was discarded, and the supernatant (SN) was
96 filtered using the Thermo Scientific Nalgene Rapid-Flow 75 mm Filter Unit (500 mL) to avoid
97 bacterial contamination. Afterwards, the SN was concentrated by a Centricon Plus-70 10 KDa
98 system using the JS-5.3 Swinging-Bucket Rotor. To ensure free contamination during the process,
99 an extra step of 0.22 µm filtration was added to the protocol. The filtered and concentrated SN
100 was then ultra-centrifuged in a Beckman Coulter optima L-100 XP ultracentrifuge using the
101 SW41 Ti Swinging-Bucket Rotor at 154,300 x g for 2h and at 4°C to precipitate the EVs. The
102 pellet containing the isolated *C. acnes* EVs was washed with 1X phosphate buffered-saline (PBS)
103 buffer and ultra-centrifuged again for 1h under the same conditions as in the previous step.

104 Finally, the SN was discarded, and the pellet was resuspended with 200 µL of PBS buffer and
105 kept in an Eppendorf at −20°C. To ensure non-bacterial presence in EVs samples, 10 µL of each
106 batch were seeded in a Brucella agar plate and incubated for 4-5 days at 37°C under anaerobic
107 conditions.

108 **2.3 EVs labelling protocol**

109 EVs labelling was performed as previously described by (Bajic et al., 2020; Cañas et al., 2016;
110 Fábrega et al., 2017). Briefly, isolated A1 EVs were resuspended in PBS buffer, centrifuged at
111 154,300 x g for 2h at 4°C, and resuspended in labelling buffer (50 mM Na_2CO_3, 100 mM NaCl,
112 pH 9.2) in the presence of 1 mg/mL of octadecyl rhodamine B-R18 (Invitrogen) and incubated
113 for 1 h at 25°C. Labelled A1 EVs were pelleted by ultracentrifugation at 154,300 x g for 1h at
114 4°C, resuspended in PBS buffer (0.2 M NaCl) and washed three times to fully remove the
115 unbound dye. After the final ultracentrifugation step, B-R18 labelled A1 EVs were resuspended
116 in PBS buffer (0.2 M NaCl) containing a protease inhibitory cocktail (Complete Protease
117 Inhibitory Tablets, Roche) and were stored at -20°C.

118 **2.4 Negative staining and Transmission Electron Microscopy (TEM)**

119 Isolated *C. acnes* H1 EVs were examined by TEM after negative staining, as described in previous
120 publications (Aguilera et al., 2014). In this particular case, EVs were resuspended in TRIS buffer
121 as PBS buffer is not compatible with uranyl acetate. A drop of EVs suspension was absorbed for
122 2 min on Formvar/carbon-coated grids that were previously activated with UV light. The grids
123 were washed with distilled water, stained with 2% uranyl acetate for 1 min, air dried and examined
124 by TEM (*Parc Científic de Barcelona*).

125 **2.5 Nanoparticle Tracking Analysis (NTA) of EVs**

126 EVs resuspended in 200 µL of PBS buffer were sent to *Institut de Ciència de materials de*
127 *Barcelona* to be examined with the Malvern Nanosight NS300 instrument. This system uses NTA

128 technology characterize nanoparticles in suspension in the size range of 10-2000 nm. A video is
129 taken and the NTA software tracks the Brownian motion of individual EVs and calculates their
130 size and total concentration.

131 **2.6 Determination of protein concentration and SDS-PAGE**

132 Protein concentrations in EVs samples were determined using the Qubit Protein Assay Kit
133 (Thermo Fisher Scientific). Measuring was done using the Qubit Fluorometer (Thermo Fisher
134 Scientific). This assay was performed at room temperature using specific Qubit assay tubes (Cat.
135 no. Q32856).

136 For protein separation, the samples were subjected to sodium dodecyl sulfate-polyacrylamide gel
137 electrophoresis (SDS-PAGE) using the Mini Gel Tank electrophoresis system (Invitrogen).
138 Proteins were denatured in a loading buffer (4X LDS sample buffer + β -mercaptoethanol) at
139 98°C for 5 min. Then, 10 µL of PageRuler Protein Ladder and 7 µg of each sample of proteins
140 mixed with 5 µL of loading buffer were loaded and separated on a NuPAGE 4 to 12% Bis-Tris
141 Gel (Invitrogen) using MOPS SDS Running Buffer 20X (Life technologies) at a constant voltage
142 of 100 V and for 40 min. After the run was completed, several bands were identified. Gel images
143 were visualized in the ChemiDoc MP Imaging System (Bio-Rad).

144 **2.7 Proteomic analysis: EVs preparation**

145 EVs were lysed to get a total representation of their protein content. To do that, liquid nitrogen
146 (N_2) was used to obtain beads of the EVs solutions of each *C. acnes* phylotype. Then, 0.5 g of
147 beads were disrupted using the Freezer Mill. Conditions used for the lysis were: precooling for 5
148 min, running step for 2 min, 2 cycles of interval and at a rate of 10 cycles per second (CPS). The
149 powder obtained was resuspended in RIPA buffer supplemented with complete protease
150 inhibitory tablets (Roche). Afterwards, total protein was precipitated with acetone and the final
151 precipitate was resuspended with a quantity ranging from 50 µL to 250 µL of 6 M urea to have a

152 minimum of 8 µg of protein. Qubit protein assay was performed to determine the estimated
153 quantity of protein in each EV sample.

154 **2.8 Identification of EVs proteins by LC-MS/MS analysis**

155 For the identification of the EVs proteins, mass spectrometry was performed by the UPF/CRG
156 Proteomics Unit.

157 Samples (8 µg) were reduced with dithiothreitol (24 nmol, 37°C, 60 min) and alkylated in the
158 dark with iodoacetamide (48 nmol, 25°C, 30 min). The resulting protein extract was first diluted
159 to 2M urea with 200 mM ammonium bicarbonate for digestion with endoproteinase Lys-C (1:10
160 w:w, 37°C, o/n, Wako, cat # 129-02541), and then diluted 2-fold with 200 mM ammonium
161 bicarbonate for trypsin digestion (1:10 w:w, 37°C, 8h, Promega cat # V5113). After digestion,
162 the peptide mix was acidified with formic acid and desalted with a MicroSpin C18 column (The
163 Nest Group, Inc) prior to LC-MS/MS analysis.

164 Afterwards, samples were analysed using the LTQ - Orbitrap Fusion Lumos mass spectrometer
165 (Thermo Fisher Scientific, San Jose, CA, USA) coupled with an EASY-nLC 1200 (Thermo Fisher
166 Scientific (Proxeon), Odense, Denmark). Peptides were loaded directly onto the analytical
167 column and were separated by reversed-phase chromatography using a 50-cm column with an
168 inner diameter of 75 µm, packed with a 2 µm C18 particles spectrometer (Thermo Scientific).

169 Chromatographic gradients started at 95% buffer A and 5% buffer B with a flow rate of 300
170 nL/min for 5 min and gradually increased to 25% buffer B and 75% A in 79 min and then to 40%
171 buffer B and 60% A in 11 min. After each analysis, the column was washed for 10 min with 10%
172 buffer A and 90% buffer B. Buffer A: 0.1% formic acid in water. Buffer B: 0.1% formic acid in
173 80% acetonitrile.

174 The mass spectrometer was operated in positive ionization mode with nanospray voltage set at
175 2.4 kV and source temperature at 305°C. The acquisition was performed in data-dependent

176 acquisition (DDA) mode and full MS scans with 1 micro scan at a resolution of 120,000 were
177 used over a mass range of m/z 350-1400 with detection in the Orbitrap mass analyser, auto gain
178 control (AGC) was set to "Standard" and maximum injection time to "Auto". In each cycle of
179 data-dependent acquisition analysis, following each survey scan, the most intense ions above a
180 threshold ion count of 10000 were selected for fragmentation. The number of selected precursor
181 ions for fragmentation was determined by the "Top Speed" acquisition algorithm and a dynamic
182 exclusion of 60 seconds. Fragment ion spectra were produced via high-energy collision
183 dissociation (HCD) at a normalized collision energy of 28% and they were acquired in the ion
184 trap mass analyser. AGC was set to 2E4, and an isolation window of 0.7 m/z and a maximum
185 injection time of 12 ms were used. Digested bovine serum albumin (New England Biolabs cat #
186 P8108S) was analysed between each sample to avoid sample carryover and to assure stability of
187 the instrument and QCloud (Chiva et al., 2018) has been used to control instrument longitudinal
188 performance during the project.

189 Acquired spectra were analysed using the Proteome Discoverer software suite (v2.0, Thermo
190 Fisher Scientific) and the Mascot search engine (v2.6, Matrix Science (Perkins et al., n.d.)). The
191 data were searched against NCBI *acnes* phylotype H2171202 database (as in August 2021, 2476
192 entries, https://www.ncbi.nlm.nih.gov/nuccore/NC_006085.1). For peptide identification a
193 precursor ion mass tolerance of 7 ppm was used for MS1 level, trypsin was chosen as the enzyme,
194 and up to three missed cleavages were allowed. The fragment ion mass tolerance was set to 0.5
195 Da for MS2 spectra. Oxidation of methionine and N-terminal protein acetylation were used as
196 variable modifications whereas carbamidomethylation on cysteines was set as a fixed
197 modification. The false discovery rate (FDR) in peptide identification was set to a maximum of
198 5%. Peptide quantification data were retrieved from the "Precursor ion area detector" node from
199 Proteome Discoverer (v2.0) using 2 ppm mass tolerance for the peptide extracted ion current
200 (XIC). The obtained values were used to calculate protein fold changes and their corresponding
201 adjusted p values.

202 **2.9 Bioinformatic analysis**

203 Proteins found by mass spectrometry were annotated from the UniProt database (UniProt
204 Consortium, 2021). Pseudo proteins or proteins lacking information in UniProt were removed
205 from the analysis. Only proteins with an area found in two or three of the replicas were considered.
206 The mean of the areas of each protein was calculated.
207
208 Proteins present only in one of the three phylotype EVs were selected for further analysis. The
209 information on biological processes, cellular components and molecular functions was obtained
210 and manually curated to classify each protein into a category.

211 **2.10 *In vitro* human cell lines maintenance**

212 The immortalized keratinocytes cell line (HaCaT), bought in the American Type Culture
213 Collection (ATCC), were cultured in T-75 culture flasks (Thermo Scientific) with Dulbecco's
214 Modified Eagle Medium (DMEM, Gibco) supplemented with 10% of Fetal Bovine Serum (FBS)
215 and 0.1% of penicillin and streptomycin. They were incubated at 37°C in 5% of CO_2, and 95% of
216 humidity until 90-100% of confluency.

217 Immortalized human SZ95 sebocytes (Zouboulis et al., 1999) were cultured in T-75 culture flasks
218 (Thermo Scientific) with Sebomed basal medium (DMEM/F12, Gibco) supplemented with 10%
219 of FBS, 0.1% of penicillin and streptomycin, 5 ng/mL of recombinant human epidermal growth
220 factor (EGFr) and 500 µL of filtrated calcium chloride ($CaCl_2$) 1M. They were incubated at 37°C
221 in 5% of CO_2, and 95% of humidity until 90-100% of confluency.

222 The immortalized T lymphocytes cell line (Jurkat, Clone E6-1), bought in the ATCC, were
223 cultured in T-75 culture flasks (Thermo Scientific) with Roswell Park Memorial Institute medium
224 (RPMI, Gibco) supplemented with 10% of FBS and 0.1% of penicillin and streptomycin. They
225 were incubated at 37°C in 5% of CO_2, and 95% of humidity until 90-100% of confluency.

226 PCi-SEB, derived from human iPSC with a Caucasian phototype (Phenocell), were seeded at a
227 density of 25.000 viable cells/cm^2 on fibronectin-coated tissue culture plate (Falcon) in

228 PhenoCULT-SEB basal medium supplemented with 0.1% of supplement A. Then, the media was
229 changed and supplemented with 0.1% of supplement M and incubated for 2 days more until cells
230 reached 90% of confluence and they were differentiated into mature sebocytes. Cells were
231 incubated at 37°C in 5% CO_2 and 95% of humidity during the whole differentiation process.

232 **2.11 Internalization of labelled-EVs**

233 To monitor EVs uptake by both HaCaT and SZ95 sebocytes, a total of $1 \cdot 10^5$ cells were seeded in
234 an 8-well chamber slider (Ibidi) until approximately 80% of confluence. Before the assay, the
235 medium was aspirated and replaced with rhodamine B-R18-labelled A1 EVs (2 µg/mL)
236 suspended in DMEM and Sebomed both without fetal bovine serum and red phenol. The cells
237 with the labelled A1 EVs were incubated at 37°C in 5% of CO_2, and 95% of humidity for 24h.

238 **2.12 Confocal fluorescence microscopy**

239 Cells were fixed for 30 min with 3% of paraformaldehyde at room temperature (RT) and washed
240 with PBS buffer to eliminate possible EVs residues. Plasma membranes were labelled with
241 fluorescent Alexa-488 wheat germ agglutinin (WGA) (Invitrogen) and nuclei with Hoechst
242 (Invitrogen). For this, cells were incubated for 25 min with Alexa-488 WGA (1 µg/mL) and
243 during 10-15 min with Hoechst (3 drops/mL). After PBS buffer washing, Ibidi mounting medium
244 was added (3 drops/well) to prepare the cells for microscopic visualisation.
245
246 Confocal microscopy was carried out using a ZEISS LSM 980 with Airyscan 2 confocal
247 microscope, using the 63x oil immersion objective lens. Fluorescence was recorded at 405 nm
248 (blue; Hoechst), 488 nm (green; WGA) and 546 nm (red; rhodamine B-R18). Z-stack images
249 were taken at 1.0-µm. Images were analysed using the Fiji image processing package.

250 **2.13 Cytotoxicity assay**

251 To evaluate cytotoxicity, an XTT Cell Viability Assay (Invitrogen) was performed following the
252 manufacturer's protocol. The assay kit includes the XTT reagent and an Electron Coupling
253 Reagent. In this case, the XTT reagent, is sensitive to cellular redox potential and in the presence
254 of live cells converts from a water-soluble compound to an orange-coloured formazan product.
255 $2 \cdot 10^5$ cells/mL of HaCaT and SZ95 sebocytes were seeded in two different 96-well plates. After
256 24h, cells were incubated with 1.56 µg/mL, 3.125 µg/mL, 6.25 µg/mL, 12.5 µg/mL, 25 µg/mL,
257 50 µg/mL, 100 µg/mL and 200 µg/mL of *C. acnes* A1, H1 and H2 EVs for 24h at 37°C in 5% of
258 CO_2 and 95% of humidity. Then, 70 µL of working solution (XTT reagent) were added directly
259 to each well. Cells were incubated for 4h at 37°C in 5% of CO_2 and 95% of humidity. After
260 incubation, the absorbance was measured in the plate reader (Tecan) at 450 nm and 660 nm to
261 eliminate the background signal contributed by cell debris or other non-specific absorbance.
262 Negative controls with non-treated cells were included as blanks.
263 The percentage of cell viability was calculated using the following formula:

264 $$\% \text{ Cell Viability} = \frac{\text{Absorbance in Test well}}{\text{Absorbance in Blank well}} \cdot 100$$

265 **2.14 *C. acnes* EVs incubation in the outer skin layer model, the sebum model and the broken**
266 **skin barrier model**

267 *C. acnes* A1, H1 and H2 EVs were incubated with the immortalized HaCaT, SZ95 sebocytes and
268 Jurkat cell lines (Fig. S2). For this purpose, $2 \cdot 10^5$ cells/mL were seeded in a 12-well plate for the
269 three cell lines. After 24h, all cell types were incubated for 24h with *C. acnes* A1, H1 and H2
270 EVs. The three plates were divided into three rows - one for each *C. acnes* phylotype - and each
271 row had a control well and different concentrations of EVs, namely 12.5 µg/mL, 25 µg/mL and
272 50 µg/mL.

273 **2.15 Quantitative Real Time-PCR analysis (RT-qPCR)**

274 Total RNA was extracted from HaCaT, SZ95 sebocytes and Jurkat cells using the miRNeasy Mini
275 Kit (Qiagen) following the manufacturer's recommendations. Purity and RNA concentration were
276 measured by the absorbance ratio at 260 and 280 nm on the NanoDrop One spectrophotometer
277 (Thermo Scientific).

278 RNA was reverse transcribed using the cDNA Reverse Transcription Kit (Thermo Fisher
279 Scientific) in a final volume of 20 µL following the manufacturer's protocol. The retro
280 transcription reaction was performed in the ProFlex PCR System (Applied Biosystems). RT-
281 qPCR reactions were performed on the QuantStudio 7 Flex Real-Time PCR System (Applied
282 Biosystems) using SYBR Green PCR Master Mix (Applied Biosystems) and cell-type specific
283 primers. See the list of primers in Table S4 of the Supporting Information. A control reaction was
284 set up with water in which no RNA was present. The $2^{-\Delta\Delta Ct}$ method was used to normalise
285 expression results. The values of the housekeeping CREBBP gene were used to standardise the
286 values obtained for each of the genes being studied.

287 **2.16 Multiplex panel (Eve Technologies)**

288 To validate the results obtained in the RT-qPCR, a Human High Sensitivity Plex Discovery Assay
289 was performed (Eve Technologies). The targets of interest were selected from an extensive list of
290 analytes and the company allowed multiplexing the previously selected targets together in a single
291 assay. Among all the analytes, the ones that stood out for us in the present project were cytokines
292 and chemokines.

293 **2.17 Evaluation of sebum-reducing potential of *C. acnes* A1, H1 and H2 EVs in the acne-**
294 **mimicking skin model**

295 For the acneic model, human iPSC-derived sebocytes (PCi-SEB) were incubated for 5 days with
296 maturation supplement. After that, the sebum production was induced by 48h of treatment with 5
297 µM of arachidonic acid (AA5). Then, cells were treated with 12.5 µg/mL of *C. acnes* A1, H1 and
298 H2 EVs for 24h and cells were fixed until sebum production determination. In parallel, non-

299 treated cells were used as negative control. For lipid droplets detection, cells were stained with
300 the fluorescent marker BODIPY 493/503 (Sigma Aldrich) following manufacture's
301 recommendations. The nucleus was stained with DAPI. Samples were analysed by confocal
302 fluorescence microscopy.

303 **2.18 Statistical analyses**

304 Statistical analyses were performed with GraphPad software. All tests were repeated
305 independently at least three times in triplicate. The values for all measurements are presented as
306 the mean ± standard deviation (SD). Differences between more than two groups were assessed
307 using one-way or two-way ANOVA followed by Dunnett's test. Data with a p value less than
308 0.05 and less than 0.001 were considered statistically significant and statistically highly
309 significant, respectively.

310 **3. RESULTS**

311 **3.1 Isolation and visualization of *C. acnes* EVs**

312 *C. acnes* H1 EVs were isolated from cell-free culture supernatants (Fig. 1) and evaluated by
313 negative stain-TEM. Images displayed spherical vesicles approximately 70-100 nm in diameter
314 (Fig. 2A). To validate the TEM results and to obtain additional information, NTA which is a more
315 precise imaging technique, was carried out in *C. acnes* A1, H1 and H2 EVs. This last analysis
316 provided high-resolution particle size distribution profiles and also concentration measurements.
317 Fig. 2B shows the size distribution graphs of the different *C. acnes* EVs. On the other side, values
318 obtained after NTA revealed that H2 EVs have the largest mean vesicle size. However, in terms
319 of concentration, A1 is the phylotype with the highest EV secretion yield rate ($3.92 \cdot 10^{12}$
320 EVs/mL). Moreover, recordings of the different types of *C. acnes* EVs were acquired from the
321 NTA analysis (see Videos).

322 **3.2 Proteomic analysis comparison between *C. acnes* A1, H1 and H2 EVs**

323 SDS-PAGE analysis showed that EV triplicates of each phylotype display similar protein profiles
324 with slight differences (Fig. 3A), which is consistent with the suggested variability of protein
325 cargo between batches (Gandham et al., 2020; Hartjes et al., 2019a, 2019b; Paganini et al., 2019).
326 Furthermore, it should be noted that, although the same amount of protein was loaded into the gel
327 for the EVs of each phylotype (7 µg), the diversity of proteins is much higher in A1 EVs (clade
328 IA1) than in H1 and H2 EVs (clade IB). These findings are in line with the ones obtained by
329 Chudzik et al.
330 To characterize the protein profile of *C. acnes* A1, H1 and H2 EVs, the protein content was
331 isolated and examined by mass spectrometry by the UPF/CRG Proteomics Facility. As Fig. 3B
332 illustrates in a Venn diagram, the three phylotypes share 382 proteins. Additionally, a pairwise
333 comparison was performed, and the results showed that A1 and H1 share 171 proteins, A1 and
334 H2 share 66 proteins and H1 and H2 share 72 proteins.
335 Finally, observing the proteins exclusive to each phylotype it is shown that A1 EVs have the
336 highest number of high-confidence proteins identified, namely 396, followed by H1 and H2 EVs.
337 Using the UniProt database, a Gene Ontology (GO) and bioinformatics analysis were conducted
338 (Fig. 3C). In terms of biological processes, *C. acnes* A1 EVs were significantly enriched in
339 proteins participating in biosynthetic processes (22.77%) and metabolic processes (20.98%).
340 Regarding the molecular functions, binding (19.64%), transferase activity (14.29%) and
341 hydrolase activity (8.48%) were the most prevalent. For biological processes, proteins linked to
342 *C. acnes* H1 EVs were significantly enriched in transport (27.69%) and metabolic processes
343 (13.85%). Regarding the molecular functions, transporter activity (21.54%) and binding (16.92%)
344 were noteworthy. The predominant proteins involved in the biological processes of *C. acnes* H2
345 EVs were linked to transport (18.18%) and response to stimulus (9.09%). Regarding the
346 molecular functions of the vesicular proteins found in this phylotype, transporter activity
347 (27.27%), and oxidoreductase activity (18.18%) were the most prevalent. For all three types of
348 EVs, in terms of cellular components, the highest percentage of proteins were membrane-
349 associated proteins, followed by cytoplasmic proteins. Also, approximately 6-18% of the total
350 number of proteins were not properly classified as they were unknown or poorly characterized.

351 The identified proteins in *C. acnes* A1, H1 and H1 EVs are listed respectively in Tables S1, S2
352 and S3 of the Supporting Information.

353 **3.3 EVs from *C. acnes* A1 phylotype are internalized into keratinocytes and sebocytes**

354 *C. acnes* EVs internalization in HaCaT keratinocytes and SZ95 sebocytes was confirmed by
355 confocal fluorescence microscopy at 24h of incubation with rhodamine B-R18-labeled A1 EVs
356 (2 µg/ well). Membranes were labelled with WGA and nuclei with Hoechst. As anticipated, no
357 red signal was observed in untreated control cells (Fig. 4).

358 **3.4 From a concentration of 50 µg/mL and below, *C. acnes* EVs do not appear to affect cell**
359 **viability in the two different skin models tested**

360 A cytotoxicity assay was performed in HaCaT and SZ95 cells. In both tests, *C. acnes* A1, H1 and
361 H2 EVs were added at different doses (1.56 µg/mL, 3.125 µg/mL, 6.25 µg/mL, 12.5 µg/mL, 25
362 µg/mL, 50 µg/mL, 100 µg/mL and 200 µg/mL). As is shown in Fig. 5A, in the HaCaT model cell
363 viability is not reduced in any condition.
364 On the other hand, in the SZ95 model cell viability is reduced to 50-70% when concentrations of
365 200 µg/mL and 100 µg/mL of EVs are added (Fig. 5B). Nonetheless, in this model when adding
366 concentrations of 50 µg/mL and below, viability is lowered by approximately 15-20% in A1 and
367 H2 EVs but is maintained nearly at 100% in H1 EVs.

368 **3.5 EVs released by *C. acnes* A1, H1 and H2 phylotypes modulate differently the expression**
369 **of biomarkers related to the immune system, oxidative stress, skin barrier and sebum**
370 **production**

371 Different *in vitro* skin models were used to evaluate the immunomodulatory properties of direct
372 stimulation with a range of concentrations of *C. acnes* A1, H1 and H2 EVs (Fig. 1B). In this
373 sense, HaCaT, SZ95 and Jurkat immortalized cell lines were used(Colombo et al., 2017; Hewitt
374 et al., 2013; Kühbacher et al., 2017; Luongo et al., 2014; Nikolakis et al., 2015; Sutterby et al.,

375 2022; Törőcsik et al., 2021). In all *in vitro* models, cells were stimulated with *C. acnes* EVs for
376 24h, and after that, the expression level of different regulatory genes (immune system, skin barrier
377 and oxidative stress) was measured by RT-qPCR. As Fig. 6A shows, A1 EVs trigger a higher
378 stimulation of the pro-inflammatory cytokines Interleukin-8 (IL-8) and TGFβ-1, and the
379 prostaglandin COX-2 which is linked to oxidative stress, compared to H1 or H2 EVs. Regarding
380 genes involved in the reinforcement of the skin barrier, such as occludin, all concentrations of H2
381 EVs and high concentrations of H1 EVs (25 µg/mL and 50 µg/mL) were the only ones able to
382 induce a significant increase in the mRNA expression compared to the negative control. However,
383 for claudin-1, all the conditions seem to activate the expression of this gene, except low doses of
384 H2 EVs, compared to untreated cells. In contrast, expression levels of MMP-2, a matrix
385 metalloproteinase implicated in tissue remodelling (Manuel & Gawronska-Kozak, 2006), did
386 not show marked differences for any of the EVs treatment with respect to the control. Regarding
387 the skin immune system model, as Fig. 6B shows, only A1 EVs triggered a significant expression
388 of the pro-inflammatory cytokine IL-8 compared to the control, while only H1 EVs and high
389 doses of H2 EVs (50 µg/mL) had substantial anti-inflammatory cytokine IL-10 expression.
390 However, for the pro-inflammatory TNFα expression, none of the EVs conditions tested were
391 able to modulate its mRNA levels. As illustrated in Fig. 6C, A1 EVs are constantly triggering
392 greater activation of the inflammatory cytokine IL-8. Otherwise, for the sebum regulator gene
393 PLIN-2 none of the EVs tested were able to substantially stimulate the up-regulation of this gene
394 expression compared to the untreated control.

395 **3.6 EVs derived from *C. acnes* A1 phylotype induce a higher secretion of**
396 **immunomodulatory mediators in three *in vitro* skin models compared to EVs from *C. acnes***
397 **H1 and H2 phylotypes**

398 To confirm the immunomodulatory effects assayed by RT-qPCR in HaCaT, Jurkat and SZ95 *in*
399 *vitro* models, after 24h of incubation with different concentrations of A1, H1 and H2 EVs, the

400 protein secretion levels of some cytokines released in the SN were evaluated by Human High
401 Sensitivity Plex Discovery Assay (Eve Technologies).
402 As shown in Fig. 7A in the HaCaT *in vitro* model, and following the same pattern as for IL-8
403 expression level, A1 EVs displayed the highest secretion of IL-8, IL-6, TNFα and GM-CSF
404 compared to the rest of the EVs, especially when high concentrations of EVs were applied to the
405 keratinocytes. Only 25 and 50 µg/mL for H1 EVs and 50 µg/mL for H2 EVs were able to induce
406 a significant difference in IL-6 secretion compared to the negative control. In the immune system
407 model, composed of Jurkat cells (Fig. 7B), high doses of A1 EVs were observed to trigger
408 increased secretion of IL-8, IL-6 and TNFα compared to the other conditions, but in the case of
409 GM-CSF, H1 and H2 EVs were the ones involved in the activation of this factor. Regarding the
410 SZ95 model (Fig. 7C), IL-8 stimulation correlates with the gene expression data obtained
411 previously. Overall, it can be observed that A1 EVs consistently trigger significant activation of
412 the inflammation-related factors IL-8, IL-6, TNFα and GM-CSF, compared to the negative
413 control. In the case of H1 EVs, only 25 and 50 µg/mL were able to induce significant IL-8 release
414 compared to control.

415 **3.7 *C. acnes* H1 EVs showed to have a better skin sebum inhibition mechanism compared**
416 **to A1 and H2 EVs**

417 The acneic *in vitro* model consisted of a 48-hour treatment with AA5 as a sebum inducer followed
418 by a 24-hour treatment with 12.5 µg/mL of *C. acnes* A1, H1 and H2 EVs. After AA5 incubation,
419 a strong and significant increase in lipid level by about 263-fold was observed, compared to the
420 negative control condition. When PCi-SEB were treated for 24h with 12.5 µg/mL of *C. acnes* A1,
421 H1 and H2 EVs, they showed a 2.8, 4.3 and 3.6-fold reduction *versus* the AA5 condition,
422 respectively. However, although results showed that the three types of EVs had a significant
423 inhibitory effect on sebum production compared to the positive control, the best sebum inhibitory
424 effect was obtained after H1 EVs treatment, with about 4-fold inhibition compared to AA5
425 condition (Fig. 8).

426 **4. DISCUSSION**

427 The Gram-positive bacterium *C. acnes* is one of the main representative genera presents in the
428 human skin microbiota with a key and pivotal role in maintaining a healthy skin barrier. In the
429 same way that occurs in the intestine, communication between C. acnes and host cells it is
430 proposed to be *established* via soluble mediators and EVs that can diffuse through the different
431 layers of the skin (epidermis, dermis and hypodermis). Specifically, EVs act as nano-carriers of
432 proteins, metabolites and nucleic acids upon interaction and internalization into host cells.
433 Therefore, it has been suggested that, considering the cargo of *C. acnes* EVs, they will have a
434 different role, being responsible on the different effects on skin alterations. *C. acnes* strains are
435 currently classified into eight phylotypes (IA1, IA2, IB1, IB2, IB3, IC, II and III), being the IA1
436 and IA2 clades preferentially found in acne lesions whereas phylotype IB is linked to a healthy
437 skin without sign of acne. In this context, where acne vulgaris is the 8th most prevalent disease,
438 with a 9.4% world population affection and several partially effective therapeutic compounds and
439 procedures in the market (Tuchayi et al., 2015), the objective of this project has been focused on
440 studying the role of EVs secreted by A1 (IA1), H1 (IB) and H2 (IB) *C. acnes* phylotypes as a
441 safety biotherapy in cutaneous disorders such acne vulgaris.
442 EV research remains a major challenge due to their intrinsically complex biogenesis, their great
443 heterogeneity in terms of size and the natural variations between batches encountered during their
444 production (Gandham et al., 2020; Hartjes et al., 2019; Paganini et al., 2019). Nevertheless, the
445 nature (small, non-synthetic and non-replicative) of these structures makes them unique to
446 overcome important barriers found in the current dermatology and cosmetic field as it is the skin
447 penetrance, side effects derived from chemicals and maintaining the skin microbiota symbiosis.
448 However, despite this good prognose of EVs used as bio-carriers, what will determine a
449 successful, harmful or poor functionality in terms of acne vulgaris pathology, depends on the
450 specific cargo of the EVs, which is directly related to the bacterium from which they derive.
451 Therefore, as the main components are proteins, a proteomic characterization of *C. acnes* EVs
452 was performed to determine the relationship of their protein cargo with the skin microbiota. A

453 Venn diagram identified, in agreement with Chudzik et al., 2022, that A1 EVs contain the highest
454 number of proteins, in our case almost four times more proteins than in H1 EVs and nine times
455 more than in H2 EVs. These results were validated with an SDS-PAGE, where the band profile
456 was different between phylotypes (Article). This could be associated with the extra number of
457 pathogenic proteins that EVs of A1 phylotype harbour in contrast to H1 and H2 EVs. In fact,
458 McDowell A. et al, 2013 found that certain strains of *C. acnes* (specifically type IA1) were
459 capable of secreting several virulence factors that enhanced the inflammatory response. However,
460 there are no genetic studies of the *C. acnes* strains used in this work, but as it has been showed
461 previously, H1 has a protective effect against acne vulgaris development. Thus we could assume
462 that these two strains could have lost the virulence factors during evolution. Following this
463 assumption, 25 virulence factors (related to adhesion, biofilm formation, etc.) were found during
464 the mass spectrometry analysis for A1 EVs while only 2 were attributed to H1 and 0 for H2 *C.*
465 *acnes* EVs.
466 Regarding shared proteins by all the *C. acnes* EVs types, the proteomic analysis revealed that a
467 large amount of proteins related to facilitate the transfer of multiple proteins involved in
468 biochemical processes and metabolism between cells, were present in EVs, validating the carrier
469 function of these structures. Moreover, EVs are used as a way of exchange cell surface substances
470 and improve bacterial survival during infections (Chen et al., 2022), and in this sense we could
471 identify several proteins used in antibiotic resistance. These findings suggest that *C.* acnes EVs
472 are also involved in bacterial survival against external threats. In addition, due to the nature and
473 sebum oily niche of *C. acnes*, common proteins involved in lipolysis such as lysophospholipase
474 and triacylglycerol lipase, were identified in the EVs. Although these enzymes are generally
475 considered putative virulence factors, lipases are necessary for *C. acnes* to maintain healthy skin
476 by metabolizing sebum and releasing fatty acids, which are necessary to keep a proper skin acidity
477 that acts as a natural barrier against harmful pathogens, providing innate skin immunity (Kim et
478 al., 2020).
479 Considering the analysis of *C. acnes* phylotype-exclusive proteins for A1, H1 and H2 EVs,
480 important differences were found in accordance with previous studies, pointing to *C. acnes*

481 phylogroup A1 (IA1) as an acne-associated group and *C. acnes* phylogroup H1 (IB) as a beneficial
482 and skincare group (Agak et al., 2018; Choi et al., 2018b; Chudzik et al., 2022; Fitz-Gibbon
483 et al., 2013; Liu et al., 2014; Lomholt & Kilian, 2010; McLaughlin et al., 2019; Nakase
484 et al., 2021; O'Neill & Gallo, 2018; Paetzold et al., 2019). As for A1 EVs, its protein profile
485 revealed a great number of proteins involved in bacterial competition and antibiotic resistance
486 (hydrolase, Ppx/GppA phosphatase family, Metallo-ß-lactamase domain protein and histidine
487 kinase) (McLaughlin et al., 2019), biofilm formation (glycosyltransferase and serine/threonine-
488 protein kinase) and virulence (porphyrin, sialidase, HtaA domain protein, phosphoesterase,
489 hydrolase and sigma factor SigA) which were not detected in H1 or H2 EVs. Regarding the
490 exclusive proteins of H1 EVs, different proteins directly involved in fatty acid catabolism were
491 found, such as acyl-CoA dehydrogenase (Swigoňová et al., 2009) and a putative two-component
492 sensor kinase which upregulates the hydrolysis of sebum triglycerides secreting free fatty acids.
493 Indirectly, the N-acetyl-gamma-glutamyl-phosphate reductase, a protein involved in the L-
494 Arginine biosynthetic pathway was also found as part of H1 EVs. In this regard, L-arginine helps
495 to protect the skin from free radicals, increases the skin's visible hydration levels, and potentially
496 supports collagen production (Gad, 2010). All these results indicate that EVs and bacteria from
497 which they derive, share functionalities, and it point to EVs as one of the mechanisms of action
498 by which the specific *C. acnes* strains exert their effect, as it has been previously described by
499 Choi et al., 2018b or Briaud & Carroll, 2020.
500 Then, the next step in our study was to show if the presence of unique peptides in the different
501 types of *C. acnes* EVs could translate, as expected, in different functionalities in the host. For this
502 purpose, an in vitro system representing the pathophysiology derived from acne was used. During
503 acne vulgaris development, as Mattii et al., 2018 showed, not only the external skin layer is
504 affected, but sebocytes also exhibit a pivotal role. Nonetheless, unlike most of the publications
505 using skin models are based only in keratinocytes, in this work, other cell types were taken into
506 consideration, as sebocytes and immune cells, to have a closer picture of what is happening in
507 real skin during acne vulgaris. To do that, different in vitro assays were carried out. Regarding

508 cytotoxicity assays, they revealed that doses of 50 µg/mL and below of *C. acnes* EVs did not
509 appear to affect cell viability either in the HaCaT model or in the SZ95 sebocyte model, thus
510 deeming them as safe to be tested in the in vitro skin models. Comparing both cell types, it was
511 also observed that sebocytes were more responsive than keratinocytes. This can be explained
512 because sebocytes inhabit in the sebaceous gland, which is located in the dermis, protected from
513 external microbes in contrast to keratinocytes exposed and in constantly interaction with skin
514 microorganisms.
515 Then, the different EVs were directly incubated for 24h in the different in vitro models: a) the
516 outer layer skin model consisted of HaCaT cells to mimic the epidermis composed mainly of
517 keratinocytes; b) the sebum model consisted of SZ95 cells to mimic the sebaceous gland
518 environment and c) the broken barrier skin model, consisting of Jurkat cells, was chosen to get an
519 idea of when the skin barrier is disrupted, one of the severe attributes of inflammatory skin
520 diseases. The expression levels of different regulatory genes were measured by RT-qPCR and
521 results displayed that, as previously was showed by Nagy et al., 2005, in all in vitro skin models,
522 A1 EVs were systematically triggering increased activation of pro-inflammatory cytokines (Nagy
523 et al., 2005). This could be due to the presence of a large number of virulence factors found in the
524 proteomic analysis for A1 EVs. On the other side, in the broken skin barrier model, H1 EVs and
525 50 µg/mL doses of H2 EVs induced a significant expression of the anti-inflammatory cytokine
526 IL-10, reinforcing the possible protective role of these two non-pathogenic strains during acne
527 vulgaris development.
528 To cross-check the immunomodulatory effects assayed by gene expression, the protein secretion
529 levels of some cytokines released in the SN of the *in vitro* models were evaluated and it was
530 confirmed that EVs derived from *C. acnes* A1 induce a higher secretion of immunomodulatory
531 mediators in the three *in vitro* skin models compared to *C. acnes* H1 and H2 EVs. According to
532 the RT-qPCR results, it was determined that A1 EVs consistently triggered a higher activation of
533 the inflammation-related factors IL-8, IL-6, TNFα and GM-CSF, compared to H1 and H2.
534 The pathophysiology of acne includes, apart from local inflammation, a hyperproduction of
535 sebum by sebocytes which causes specific strains of *C. acnes* to overgrow causing a dysbiosis

536 and triggering the development of acne (Paetzold et al., 2019; Rozas et al., 2021). In fact, one of
537 the most prescribed treatments for dermatologists against acne is based on isotretionin, a retinoid
538 which causes the apoptosis of skin sebocytes to reduce the amount of sebum (Zouboulis, 2006).
539 However, the regulation of sebum during acne development modulated by the skin microbiota is
540 a very new topic and there are few publications on the subject. Therefore, an acneic-mimicking
541 skin model with PCi-SEB and AA5 as sebum inductor, was used to explore the effect of *C. acnes*
542 EVs on sebum regulation. After 24-hour treatment with 12.5 µg/mL of *C. acnes* A1, H1 and H2
543 EVs, results showed that the three types of EVs had a significant inhibitory effect on sebum
544 production compared to the positive control, highlighting that the best inhibition was obtained
545 after H1 EVs treatment, with inhibition by about 4 folds compared to the positive control. These
546 results were expected and in accordance with the proteomic analysis that described H1 EVs as
547 being charged with exclusive proteins with lipidomic effect.
548 To our knowledge, this is the first study in which proteomic characterization of three different
549 phylotypes of *C. acnes* has been performed, in addition to the testing of three different *C. acnes*
550 phylotypes in different *in vitro* skin models. This work has proved that *C. acnes* EVs are more
551 than lipid spheres that act as mechanisms of action of the derived bacteria. Specially H1 EVs has
552 been highlighted as the best bioactive nanocarrier, counteracting acne symptomatology from two
553 flanks, inhibiting inflammation and modulating sebum production.
554

555 **5. CONCLUSION**

556 The findings of this project have shown that *C. acnes* EVs are key intermediators in the
557 communication between skin microbiota and the host, having an essential role during skin
558 alterations such as acne vulgaris. In this sense, these results point to H1 EVs as a potential,
559 efficient, safe and based-natural treatment to prevent and ameliorate symptomatology associated
560 with inflammation and oily skin. However, further scientific experiments need to be done
561 including assays with primary cell lines, *in vivo* animal models, checking EVs stability in a gel
562 cream and performing clinical tests to extend the knowledge and to have the whole picture of how
563 *C. acnes* EVs act on the skin.

564

565 **ABBREVIATIONS**

566 *C. acnes: Cutibacterium acnes*

567 EVs: extracellular vesicles

568 PBS: phosphate-buffered saline

569 SN: supernatant

570 TEM: transmission electron microscopy

571 NTA: nanoparticle tracking analysis

572 SDS-PAGE: sodium dodecyl sulfate-polyacrylamide gel electrophoresis

573 PBS: phosphate-buffered saline

574 CPS: cycles per second

575 DDA: data-dependent acquisition

576 AGC: auto gain control

577 HCD: high-energy collision dissociation

578 FDR: false discovery rate

579 XIC: extracted ion current

580 ATCC: American Type Culture Collection

581 DMEM: Dulbecco's Modified Eagle Medium

582 FBS: Fetal Bovine Serum

583 EGFr: recombinant human epidermal growth factor

584 $CaCl_2$: calcium chloride

585 RPMI: Roswell Park Memorial Institute medium

586 RT: room temperature

587 WGA: wheat germ agglutinin

588 RT-qPCR: quantitative real time-PCR analysis

589 PCi-SEB: human iPSC-derived sebocytes

590 AA5: 5 µM of arachidonic acid

591 SD: standard deviation

592 GO: Gene Ontology

593 IL: interleukin

594 CITE: biofilm matrix dynamics

595 ETHICS APPROVAL AND CONSENT TO PARTICIPATE

596 Not applicable

597 CONSENT FOR PUBLICATION

598 All authors give their consent for publication of this work in Microbiome as a research article.

599 AVAILABILITY OF DATA AND MATERIALS

600 The raw data from proteomic analysis are included as Supporting Tables S1, S2 and S3.

601 The original R scripts for plotting the extracellular vesicle data are available on Bitbucket.
602 (https://bitbucket.org/synbiolab/fabrega_vesicles/src/master/)

603 COMPETING INTERESTS

604 The authors declare that they have not competing interests

605 FUNDING INFORMATION

606 This work was funded and supported by the University Pompeu Fabra – Excelencia Maria de
607 Maeztu Post-doctoral program (CEX 2018-0007392-M). NK is funded by a Maria Maetzu-UPF
608 fellowship (Catalan Government) and by the Sociedad Española de Químicos Cosméticos
609 (SEQC) and MJF is funded by a Juan de la Cierva Fellowship from the Spanish Government
610 (Award FJC 2018-037096-I).

611 AUTHOR'S CONTRIBUTIONS

612 M.P. participated in the experimental laboratory work, data curation, formal analysis, writing the
613 main manuscript text and preparing all figures. J.M. did the bioinformatic analysis, prepared
614 figure 3 and helped with the writing of the original draft. L.T. and N.K. participated in the
615 experimental laboratory work, specially helping to set up the in vitro assays and bacterial cultures.
616 J.M. participated in the experimental laboratory work, developing the in vitro acneic model and
617 preparing figure 8. M.G. contributed supervising the project and helping to write the main
618 manuscript text. M.F. helped with the experimental laboratory work, data curation, formal
619 analysis, writing the manuscript, doing the funding acquisition/project administration, and
620 supervising the project. C,C,Z, provided its proprietary imoortalized human sebaceous gland cell
621 line SZ95 and revised the initial version of the manuscript.

622 **ACKNOWLEDGEMENT**

623 We want to express our deepest gratitude to Dr. Bernhard Paetzold for support in culturing *C.*
624 *acnes* strains. Also, Dr. Jordi García-Ojalvo for mentoring this project. We also want to thank the
625 Office Naval Research (Award N62909-18-1-2155) for giving us the opportunity to study how to
626 work with anaerobic skin bacteria.

627 **CONFLICT OF INTEREST**

628 The authors report no conflict of interest.

629
630 **REFERENCES**
631

632 Agak, G. W., Kao, S., Ouyang, K., Qin, M., Moon, D., Butt, A., & Kim, J. (2018).
633 Phenotype and Antimicrobial Activity of Th17 Cells Induced by
634 Propionibacterium acnes Strains Associated with Healthy and Acne Skin. *Journal*
635 *of Investigative Dermatology*, *138*(2), 316–324.
636 https://doi.org/10.1016/j.jid.2017.07.842
637 Bajic, S. S., Cañas, M. A., Tolinacki, M., Badia, J., Sánchez, B., Golic, N., Margolles,
638 A., Baldomá, L., & Ruas-Madiedo, P. (2020). Proteomic profile of extracellular
639 vesicles released by Lactiplantibacillus plantarum BGAN8 and their internalization
640 by non-polarized HT29 cell line. *Scientific Reports*, *10*(1).
641 https://doi.org/10.1038/s41598-020-78920-z
642 Blum, H. E. (2017). The human microbiome. In *Advances in Medical Sciences* (Vol. 62,
643 Issue 2, pp. 414–420). Medical University of Bialystok.
644 https://doi.org/10.1016/j.advms.2017.04.005

Briaud, P., & Carroll, R. K. (2020). Extracellular vesicle biogenesis and functions in gram-positive bacteria. *Infection and Immunity*, *88*(12). https://doi.org/10.1128/IAI.00433-20/FORMAT/EPUB

Brown, L., Wolf, J. M., Prados-Rosales, R., & Casadevall, A. (2015). Through the wall: Extracellular vesicles in Gram-positive bacteria, mycobacteria and fungi. In *Nature Reviews Microbiology* (Vol. 13, Issue 10, pp. 620–630). Nature Publishing Group. https://doi.org/10.1038/nrmicro3480

Cañas, M. A., Giménez, R., Fábrega, M. J., Toloza, L., Baldomà, L., & Badia, J. (2016). Outer membrane vesicles from the probiotic Escherichia coli Nissle 1917 and the commensal ECOR12 enter intestinal epithelial cells via clathrin-dependent endocytosis and elicit differential effects on DNA damage. *PLoS ONE*, *11*(8). https://doi.org/10.1371/journal.pone.0160374

Chen, J., Zhang, H., Wang, S., Du, Y., Wei, B., Wu, Q., & Wang, H. (2022). Inhibitors of Bacterial Extracellular Vesicles. *Frontiers in Microbiology*, *13*. https://doi.org/10.3389/fmicb.2022.835058

Choi, E. J., Lee, H. G., Bae, I. H., Kim, W., Park, J., Lee, T. R., & Cho, E. G. (2018a). Propionibacterium acnes-Derived Extracellular Vesicles Promote Acne-Like Phenotypes in Human Epidermis. *Journal of Investigative Dermatology*, *138*(6), 1371–1379. https://doi.org/10.1016/j.jid.2018.01.007

Choi, E. J., Lee, H. G., Bae, I. H., Kim, W., Park, J., Lee, T. R., & Cho, E. G. (2018b). Propionibacterium acnes-Derived Extracellular Vesicles Promote Acne-Like Phenotypes in Human Epidermis. *Journal of Investigative Dermatology*, *138*(6), 1371–1379. https://doi.org/10.1016/J.JID.2018.01.007

Christensen, G. J. M., Scholz, C. F. P., Enghild, J., Rohde, H., Kilian, M., Thürmer, A., Brzuszkiewicz, E., Lomholt, H. B., & Brüggemann, H. (2016). Antagonism between Staphylococcus epidermidis and Propionibacterium acnes and its genomic basis. *BMC Genomics*, *17*(1). https://doi.org/10.1186/s12864-016-2489-5

Chudzik, A., Migdał, P., & Paściak, M. (2022). Different Cutibacterium acnes Phylotypes Release Distinct Extracellular Vesicles. *International Journal of Molecular Sciences*, *23*(10), 5797. https://doi.org/10.3390/ijms23105797

Colombo, I., Sangiovanni, E., Maggio, R., Mattozzi, C., Zava, S., Corbett, Y., Fumagalli, M., Carlino, C., Corsetto, P. A., Scaccabarozzi, D., Calvieri, S., Gismondi, A., Taramelli, D., & Dell'Agli, M. (2017). HaCaT Cells as a Reliable in Vitro Differentiation Model to Dissect the Inflammatory/Repair Response of Human Keratinocytes. *Mediators of Inflammation*, *2017*. https://doi.org/10.1155/2017/7435621

Eisenstein, M. (2020). The skin microbiome. *Nature Outlines*, *588*, S209.

Fábrega, M. J., Rodríguez-Nogales, A., Garrido-Mesa, J., Algieri, F., Badía, J., Giménez, R., Gálvez, J., & Baldomà, L. (2017). Intestinal anti-inflammatory effects of outer membrane vesicles from Escherichia coli Nissle 1917 in DSS-experimental colitis in mice. *Frontiers in Microbiology*, *8*(JUL). https://doi.org/10.3389/fmicb.2017.01274

Fitz-Gibbon, S., Tomida, S., Chiu, B. H., Nguyen, L., Du, C., Liu, M., Elashoff, D., Erfe, M. C., Loncaric, A., Kim, J., Modlin, R. L., Miller, J. F., Sodergren, E., Craft, N., Weinstock, G. M., & Li, H. (2013). Propionibacterium acnes strain populations in the human skin microbiome associated with acne. *Journal of Investigative Dermatology*, *133*(9), 2152–2160. https://doi.org/10.1038/jid.2013.21

Gad, M. Z. (2010). Anti-aging effects of L-arginine. In *Journal of Advanced Research* (Vol. 1, Issue 3, pp. 169–177). https://doi.org/10.1016/j.jare.2010.05.001

Gandham, S., Su, X., Wood, J., Nocera, A. L., Alli, S. C., Milane, L., Zimmerman, A., Amiji, M., & Ivanov, A. R. (2020). Technologies and Standardization in Research on Extracellular Vesicles. In *Trends in Biotechnology* (Vol. 38, Issue 10, pp. 1066–1098). Elsevier Ltd. https://doi.org/10.1016/j.tibtech.2020.05.012

Hartjes, T. A., Mytnyk, S., Jenster, G. W., van Steijn, V., & van Royen, M. E. (2019). Extracellular vesicle quantification and characterization: Common methods and emerging approaches. In *Bioengineering* (Vol. 6, Issue 1). MDPI AG. https://doi.org/10.3390/bioengineering6010007

Hewitt, N. J., Edwards, R. J., Fritsche, E., Goebel, C., Aeby, P., Scheel, J., Reisinger, K., Ouédraogo, G., Duche, D., Eilstein, J., Latil, A., Kenny, J., Moore, C., Kuehnl, J., Barroso, J., Fautz, R., & Pfuhler, S. (2013). Use of human in Vitro skin models for accurate and ethical risk assessment: Metabolic considerations. *Toxicological Sciences*, *133*(2), 209–217. https://doi.org/10.1093/toxsci/kft080

Jahns, A. C., & Alexeyev, O. A. (2014). Three dimensional distribution of Propionibacterium acnes biofilms in human skin. *Experimental Dermatology*, *23*(9), 687–689. https://doi.org/10.1111/EXD.12482

Kim, S. Y., Kim, M. H., Son, J. H., Kim, S. il, Yun, S. H., Kim, K., Kim, S., Shin, M., & Lee, J. C. (2020). Outer membrane vesicles produced by Burkholderia cepacia cultured with subinhibitory concentrations of ceftazidime enhance pro-inflammatory responses. *Virulence*, *11*(1), 995–1005. https://doi.org/10.1080/21505594.2020.1802193

Kühbacher, A., Sohn, K., Burger-Kentischer, A., & Rupp, S. (2017). Immune cell-supplemented human skin model for studying fungal infections. In *Methods in Molecular Biology* (Vol. 1508, pp. 439–449). Humana Press Inc. https://doi.org/10.1007/978-1-4939-6515-1_25

Liu, J., Cheng, A., Bangayan, N. J., Barnard, E., Curd, E., Craft, N., & Li, H. (2014). Draft genome sequences of Propionibacterium acnes type strain ATCC6919 and antibiotic-resistant strain HL411PA1. *Genome Announcements*, *2*(4). https://doi.org/10.1128/genomeA.00740-14

Lomholt, H. B., & Kilian, M. (2010). Population genetic analysis of Propionibacterium acnes identifies a subpopulation and epidemic clones associated with acne. *PLoS ONE*, *5*(8). https://doi.org/10.1371/journal.pone.0012277

Luongo, D., Russo, R., Balestrieri, A., Marzocco, S., Bergamo, P., & Severino, L. (2014). In vitro study of AFB1 and AFM1 effects on human lymphoblastoid Jurkat T-cell model. *Journal of Immunotoxicology*, *11*(4), 353–358. https://doi.org/10.3109/1547691X.2013.848250

Manuel, J. A., & Gawronska-Kozak, B. (2006). Matrix metalloproteinase 9 (MMP-9) is upregulated during scarless wound healing in athymic nude mice. *Matrix Biology*, *25*(8), 505–514. https://doi.org/10.1016/j.matbio.2006.07.008

Mattii, M., Lovászi, M., Garzorz, N., Atenhan, A., Quaranta, M., Lauffer, F., Konstantinow, A., Küpper, M., Zouboulis, C. C., Kemeny, L., Eyerich, K., Schmidt-Weber, C. B., Törőcsik, D., & Eyerich, S. (2018). Sebocytes contribute to skin inflammation by promoting the differentiation of T helper 17 cells. *British Journal of Dermatology*, *178*(3), 722–730. https://doi.org/10.1111/bjd.15879

McDowell, A., Nagy, I., Magyari, M., Barnard, E., & Patrick, S. (2013). The Opportunistic Pathogen Propionibacterium acnes: Insights into Typing, Human Disease, Clonal Diversification and CAMP Factor Evolution. *PLoS ONE*, *8*(9). https://doi.org/10.1371/journal.pone.0070897

McLaughlin, J., Watterson, S., Layton, A. M., Bjourson, A. J., Barnard, E., & McDowell, A. (2019). Propionibacterium acnes and acne vulgaris: New insights

from the integration of population genetic, multi-omic, biochemical and host-microbe studies. In *Microorganisms* (Vol. 7, Issue 5). MDPI AG. https://doi.org/10.3390/microorganisms7050128

Nagy, I., Pivarcsi, A., Koreck, A., Széll, M., Urbán, E., & Kemény, L. (2005). Distinct strains of Propionibacterium acnes induce selective human β-defensin-2 and interleukin-8 expression in human keratinocytes through toll-like receptors. *Journal of Investigative Dermatology*, *124*(5), 931–938. https://doi.org/10.1111/j.0022-202X.2005.23705.x

Nakase, K., Koizumi, J., Midorikawa, R., Yamasaki, K., Tsutsui, M., Aoki, S., Nasu, Y., Hirai, Y., Nakaminami, H., & Noguchi, N. (2021). Cutibacterium acnes phylogenetic type IC and II isolated from patients with non-acne diseases exhibit high-level biofilm formation. *International Journal of Medical Microbiology*, *311*(7). https://doi.org/10.1016/j.ijmm.2021.151538

Nikolakis, G., Seltmann, H., Hossini, A. M., Makrantonaki, E., Knolle, J., & Zouboulis, C. C. (2015). Ex vivo human skin and SZ95 sebocytes exhibit a homoeostatic interaction in a novel coculture contact model. *Experimental Dermatology*, *24*(7), 497–502. https://doi.org/10.1111/exd.12712

O'Neill, A. M., & Gallo, R. L. (2018). Host-microbiome interactions and recent progress into understanding the biology of acne vulgaris. In *Microbiome* (Vol. 6, Issue 1). BioMed Central Ltd. https://doi.org/10.1186/s40168-018-0558-5

Paetzold, B., Willis, J. R., Pereira De Lima, J., Knödlseder, N., Brüggemann, H., Quist, S. R., Gabaldón, T., & Güell, M. (2019). Skin microbiome modulation induced by probiotic solutions. *Microbiome*, *7*(1). https://doi.org/10.1186/s40168-019-0709-3

Paganini, C., Capasso Palmiero, U., Pocsfalvi, G., Touzet, N., Bongiovanni, A., & Arosio, P. (2019). Scalable Production and Isolation of Extracellular Vesicles: Available Sources and Lessons from Current Industrial Bioprocesses. In *Biotechnology Journal* (Vol. 14, Issue 10). Wiley-VCH Verlag. https://doi.org/10.1002/biot.201800528

Rackaityte, E., & Lynch, S. v. (2020). The human microbiome in the 21st century. In *Nature Communications* (Vol. 11, Issue 1). Nature Research. https://doi.org/10.1038/s41467-020-18983-8

Rozas, M., de Ruijter, A. H., Fabrega, M. J., Zorgani, A., Guell, M., Paetzold, B., & Brillet, F. (2021). From dysbiosis to healthy skin: Major contributions of cutibacterium acnes to skin homeostasis. In *Microorganisms* (Vol. 9, Issue 3, pp. 1–18). MDPI AG. https://doi.org/10.3390/microorganisms9030628

Shu, M., Wang, Y., Yu, J., Kuo, S., Coda, A., Jiang, Y., Gallo, R. L., & Huang, C. M. (2013). Fermentation of Propionibacterium acnes, a Commensal Bacterium in the Human Skin Microbiome, as Skin Probiotics against Methicillin-Resistant Staphylococcus aureus. *PLoS ONE*, *8*(2). https://doi.org/10.1371/journal.pone.0055380

Sutterby, E., Thurgood, P., Baratchi, S., Khoshmanesh, K., & Pirogova, E. (2022). Evaluation of in vitro human skin models for studying effects of external stressors and stimuli and developing treatment modalities. *VIEW*, *3*(2), 20210012. https://doi.org/10.1002/viw.20210012

Swigoňová, Z., Mohsen, A. W., & Vockley, J. (2009). Acyl-coA dehydrogenases: Dynamic history of protein family evolution. *Journal of Molecular Evolution*, *69*(2), 176–193. https://doi.org/10.1007/s00239-009-9263-0

Törőcsik, D., Fazekas, F., Póliska, S., Gregus, A., Janka, E. A., Dull, K., Szegedi, A., Zouboulis, C. C., & Kovács, D. (2021). Epidermal Growth Factor Modulates Palmitic Acid-Induced Inflammatory and Lipid Signaling Pathways in SZ95

Sebocytes. *Frontiers in Immunology*, *12*. https://doi.org/10.3389/fimmu.2021.600017

Tuchayi, S. M., Makrantonaki, E., Ganceviciene, R., Dessinioti, C., Feldman, S. R., & Zouboulis, C. C. (2015). Acne vulgaris. *Nature Reviews Disease Primers 2015 1:1*, *1*(1), 1–20. https://doi.org/10.1038/nrdp.2015.29

Zouboulis, C. C. (2006). Isotretinoin revisited: Pluripotent effects on human sebaceous gland cells. In *Journal of Investigative Dermatology* (Vol. 126, Issue 10, pp. 2154–2156). Nature Publishing Group. https://doi.org/10.1038/sj.jid.5700418

Zouboulis, C. C., Seltmann, H., Neitzel, H., & Orfanos, C. E. (1999). Establishment and characterization of an immortalized human sebaceous gland cell line (SZ95). *Journal of Investigative Dermatology*, *113*(6), 1011–1020. https://doi.org/10.1046/J.1523-1747.1999.00771.X

FIGURES AND FIGURE LEGENDS

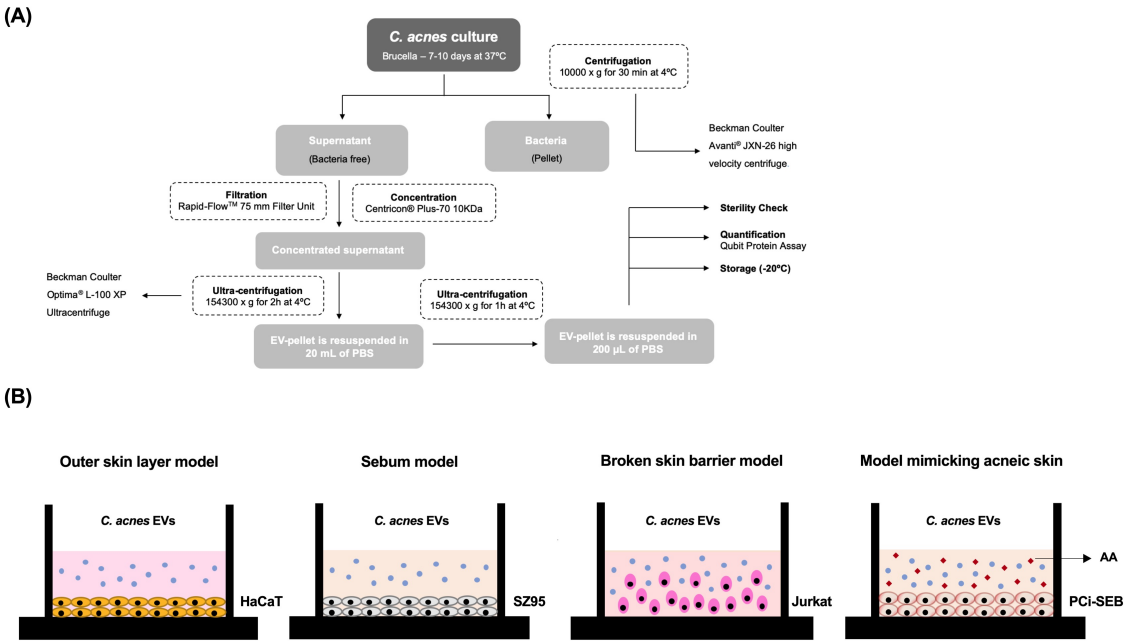

Fig. 1. **EVs isolation protocol and *in vitro* experimental design**. (A) Process to isolate C. acnes-derived extracellular vesicles (EVs). (B) Schematic presentation of the different skin in vitro

models: the outer skin layer model with HaCaT cell line, the sebum model with SZ95 sebocyte cell line, the broken skin barrier model with Jurkat cells and the acneic skin model with PCi-SEB cells using AA to induce sebum production.

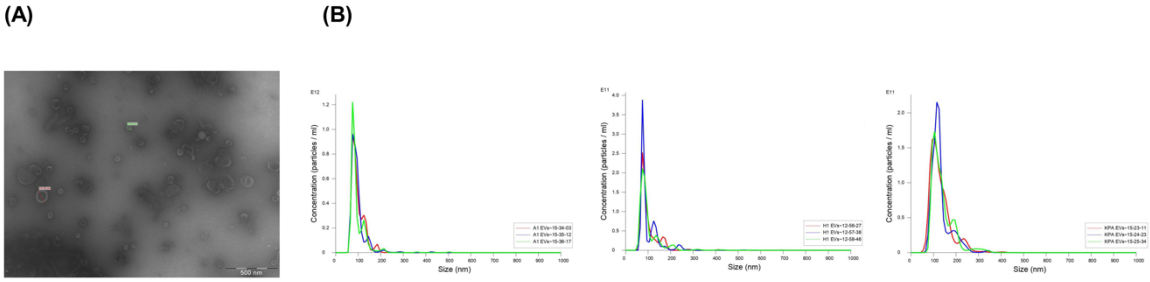

Fig. 2. Visualization of *C. acnes* EVs by different microscopy techniques. (A) Transmission Electron Microscopy of C. acnes H1 EVs (bar 500 nm). (B) Nanoparticle Tracking Analysis of *C. acnes* A1, H1 and H2 EVs. Prior to the measurement, the samples were diluted in PBS buffer at 1:5000, 1:1000 and 1:1000 respectively. EVs have a mean diameter of 96.8 ± 0.5 nm, 100.7 ± 0.7 nm and 133.0 ± 2.3 nm respectively. EV-concentration is expressed as a number of particles per mL on the y axis. All data represent the mean of three independent experiments ± standard error.

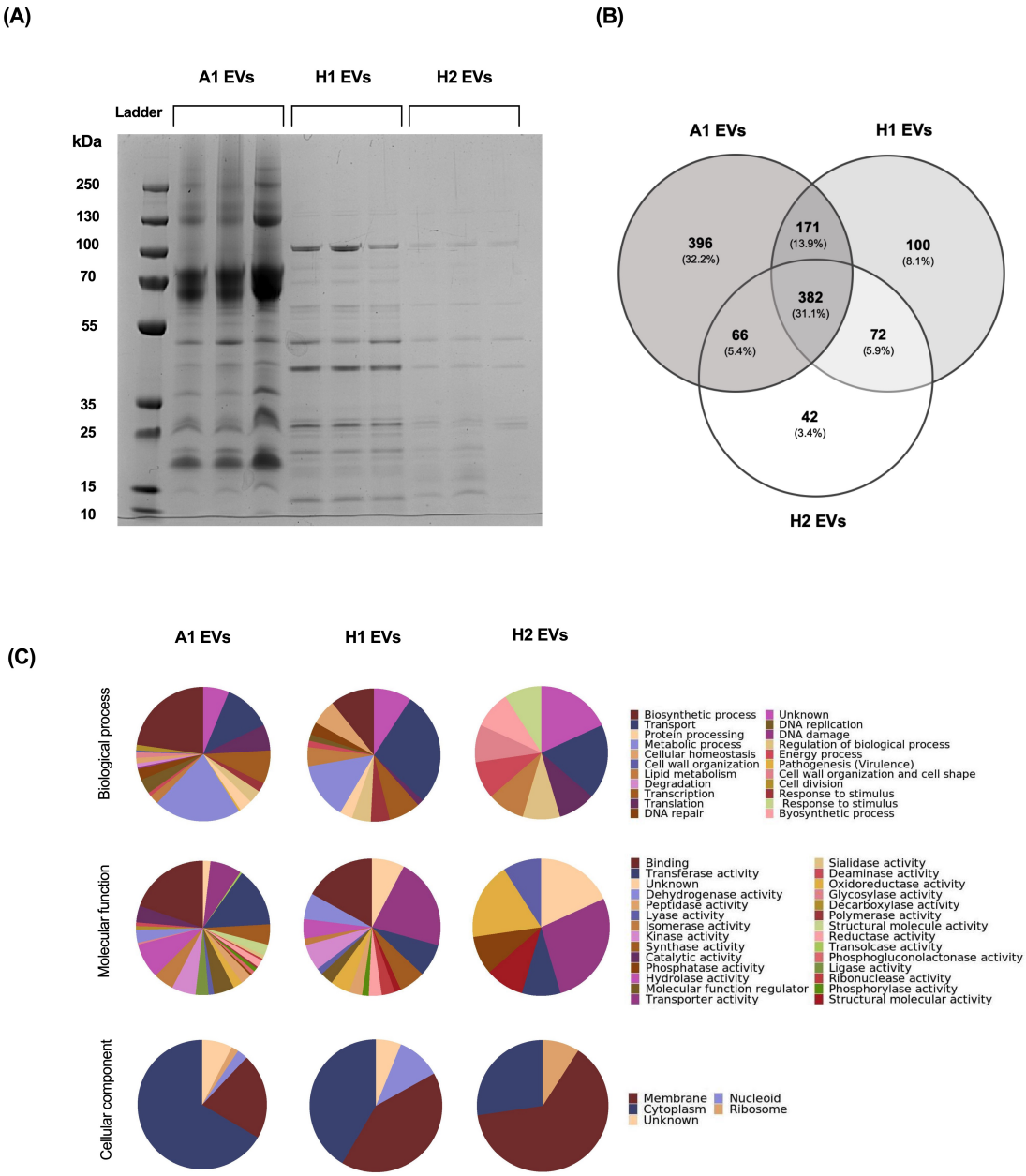

Fig. 3. Proteomic characterization of *C. acnes* A1, H1 and H2 EVs. (A) Proteomic fingerprint of *C. acnes* EVs. SDS-PAGE gel showing protein bands of triplicates from EVs of different phylotypes. A concentration of 7 µg of total amount of protein was loaded in a NuPage 4 to 12% Bis-Tris gel and stained with Coomassie Brilliant Blue R-250 staining solution. (B) Venn diagram of the proteins contained in *C. acnes* A1, H1 and H2 EVs. The number of overlapping proteins between the different phylotypes is indicated. All data is obtained from three independent experiments. (C) Gene Ontology analysis of *C. acnes* A1, H1 and H2 EVs preparations. Biological process, Molecular function and Cellular components of the identified vesicular proteins in *C. acnes* EVs are presented here. For each *C. acnes* phylotype, three independent batches were analysed in the proteomic analysis.

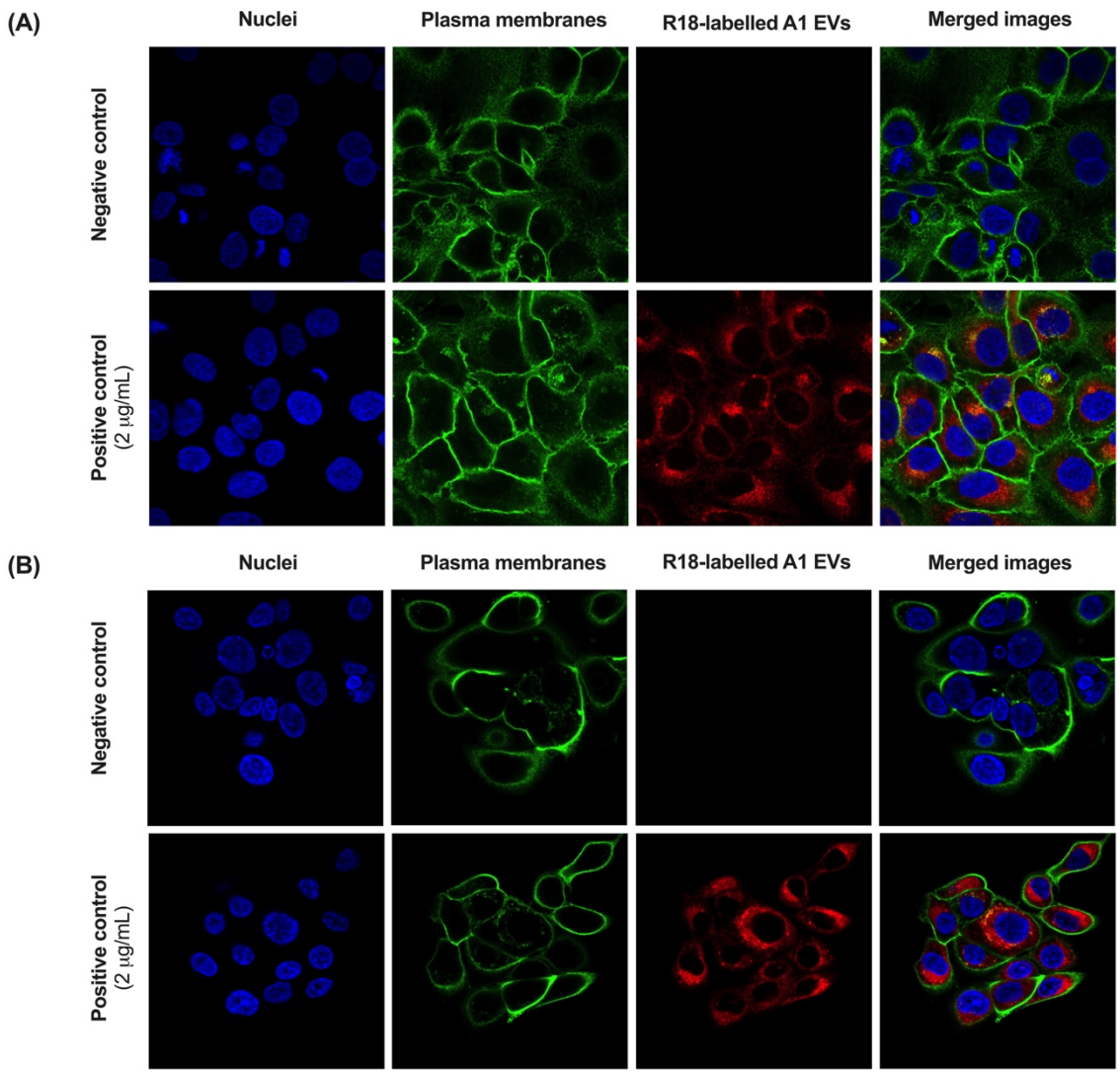

Fig. 4. Uptake of *C. acnes* A1 EVs in (A) HaCaT cell line and (B) SZ95 cell line. Visualization of internalized EVs by confocal fluorescence microscopy. Both cell lines were incubated for 24h at 37°C with rhodamine B-R18-labelled A1 EVs (2 µg/ well).

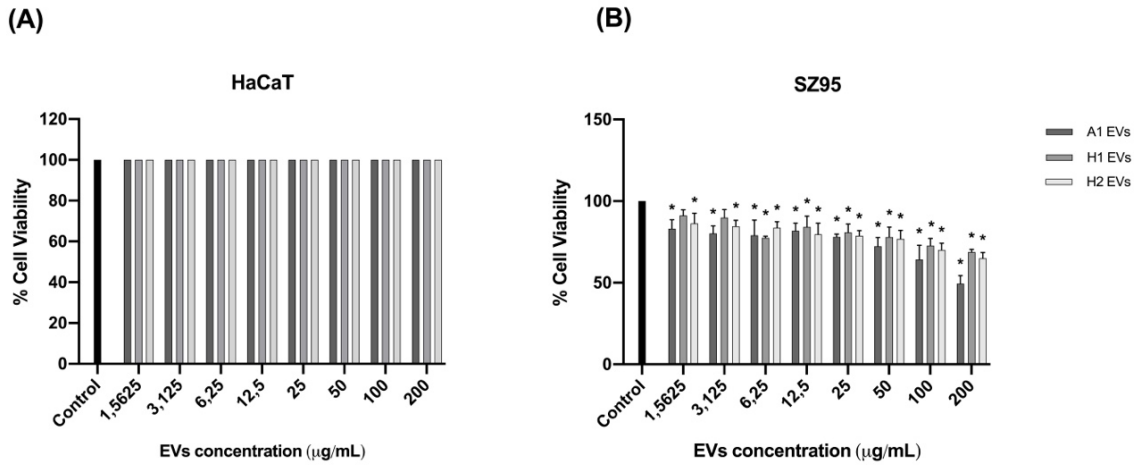

858
859

860 **Fig. 5. Cytotoxicity assay** of (A) HaCaT cell line and (B) SZ95 sebocyte cell line treated with
861 different doses of *C. acnes* A1, H1 and H2 EVs. All data are presented as mean ± standard
862 deviation (SD) of triplicate measurements (*$p \leq 0.05$ versus non-stimulated controls).

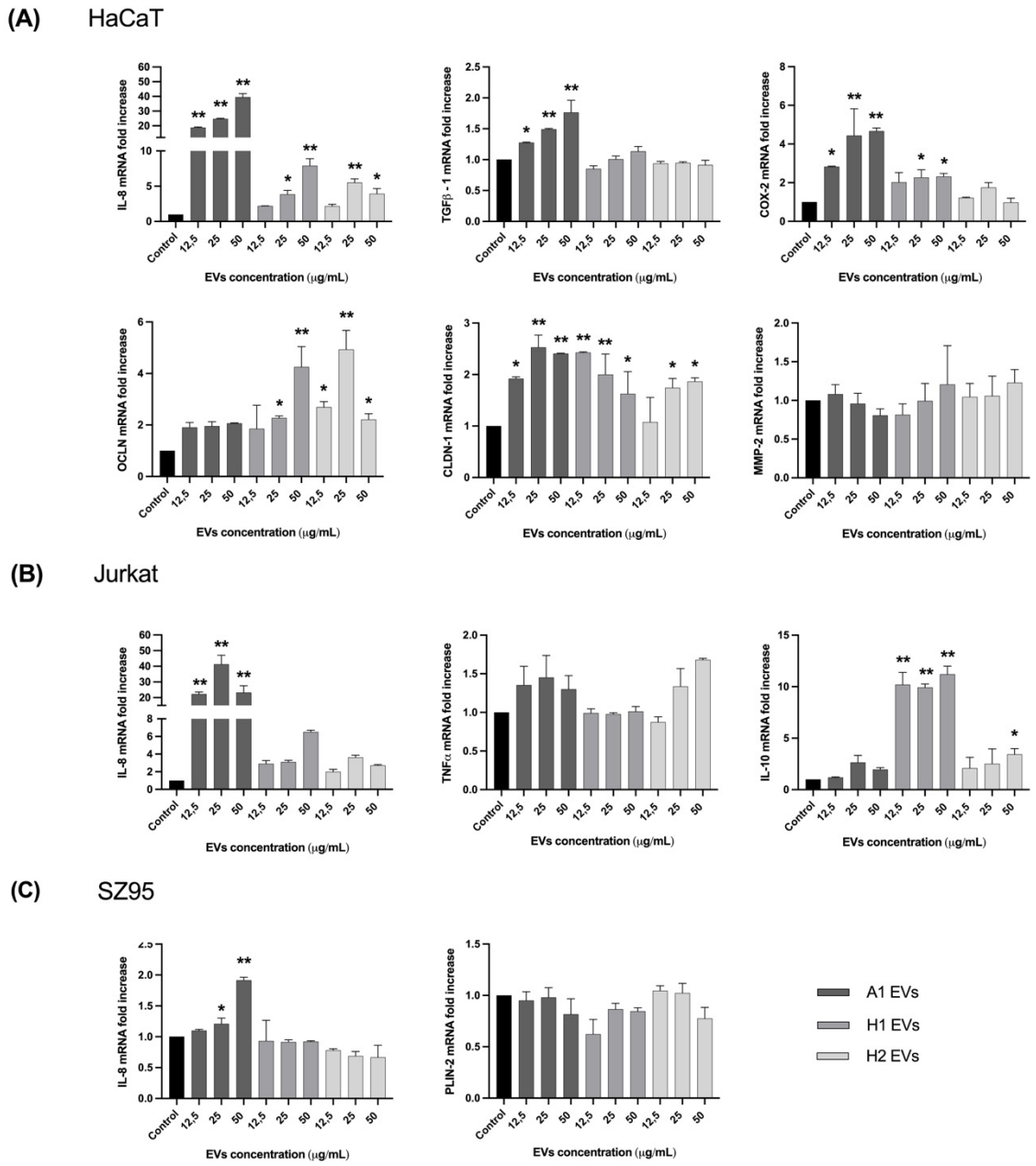

Fig. 6. *In vitro* analysis with direct incubation of *C. acnes* EVs. Human cells were treated for 24h with different concentrations (12.5, 25 and 50 µg/mL) of *C. acnes* A1, H1 and H2 EVs. Total RNA was extracted and different biomarkers were assessed by RT-qPCR. (A) HaCaT (B) SZ95 and (C) Jurkat immortalized cell lines. All data are presented as mean ± standard deviation (SD) of triplicate measurements (*$p \leq 0.05$, **$p \leq 0.001$ versus non-stimulated controls).

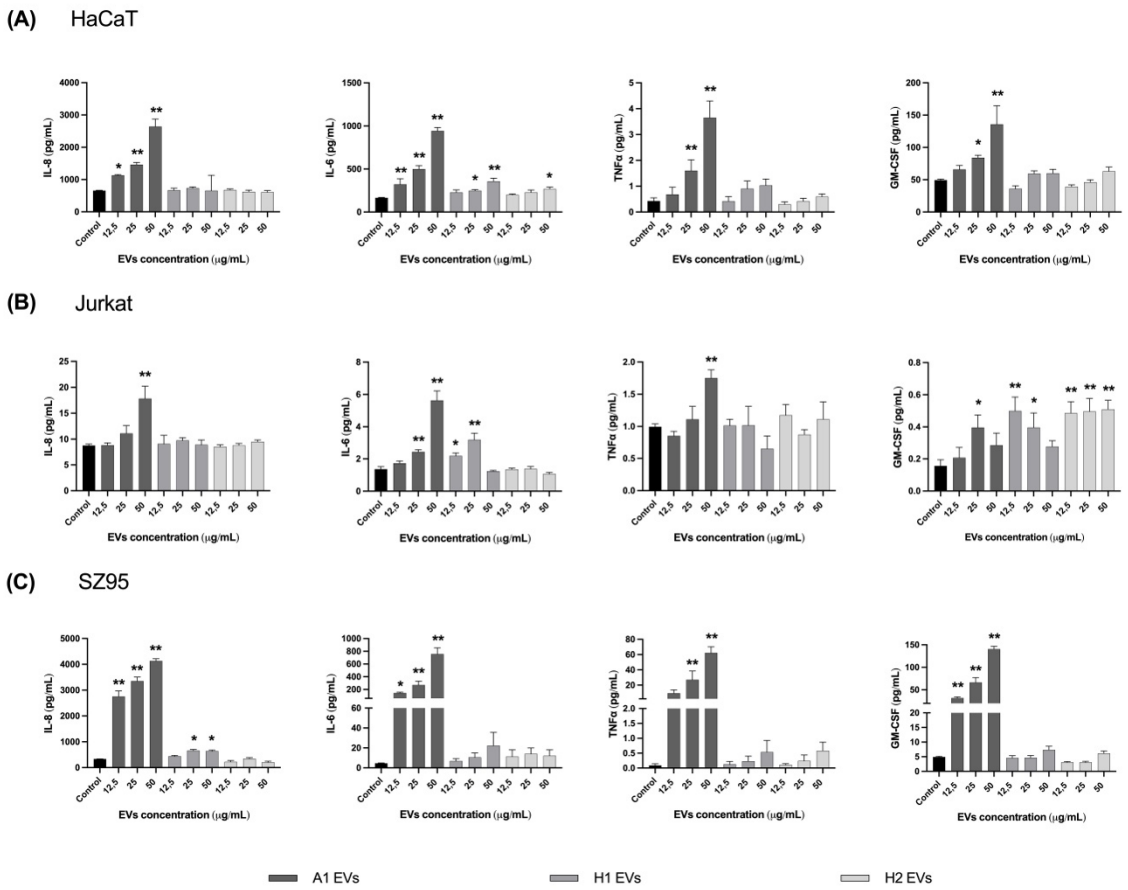

Fig. 7. Total protein concentration secreted into the SN after direct incubation with *C. acnes* EVs. Human cells were treated for 24h with different concentrations (12.5, 25 and 50 µg/mL of *C. acnes* A1, H1 and H2 EVs. Filtered SN was evaluated by Multiplex analysis to measure protein secreted in it. Ranges for the standard curve for each of the biomarkers were: GM-CSF: 0.31 - 4978.62 pg/mL, TNF alpha: 0.11 - 1699.58 pg/mL and IL-6: 0.05 - 768.83 pg/mL. (A) HaCaT (B) SZ95 and (C) Jurkat immortalized cell lines were used. All data are presented as mean ± standard deviation (SD) of triplicate measurements (*$p \leq 0.05$, **$p \leq 0.001$ versus non-stimulated controls).

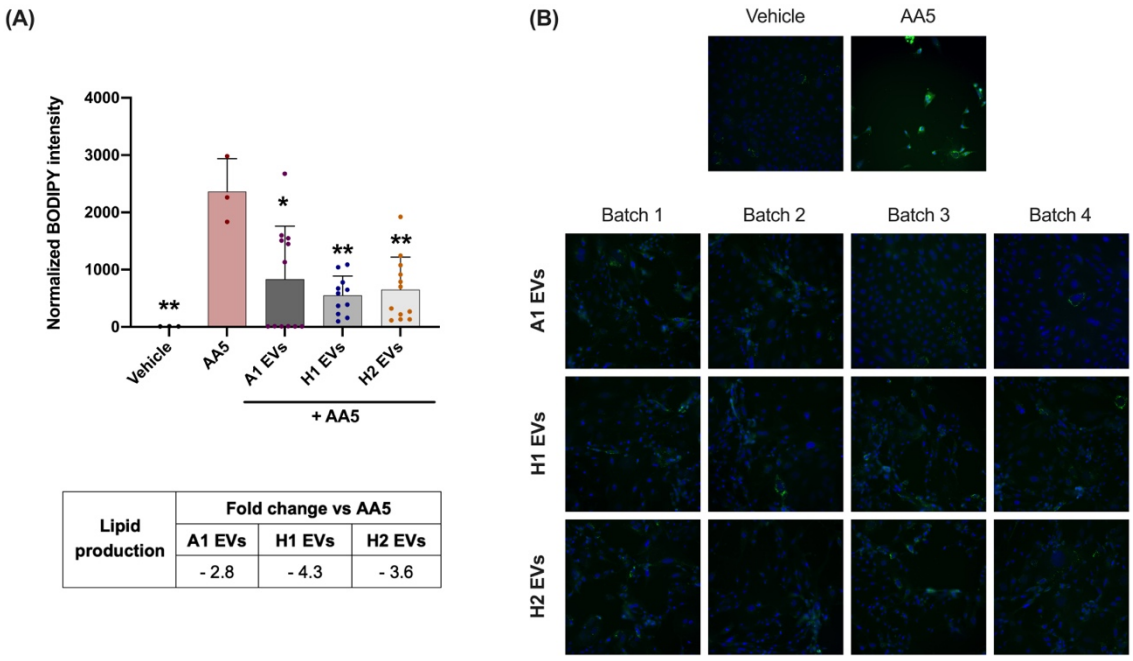

Lipid production	Fold change vs AA5		
	A1 EVs	H1 EVs	H2 EVs
	- 2.8	- 4.3	- 3.6

Fig. 8. Reduction of lipid production was assessed after treating PCi-SEB with AA5 for 24h. PCi-SEB were treated during 48h with AA at 5 µM (AA5) to induce lipid production. Afterwards PCi-SEB were treated for 24h with 12.5 µg/mL of *C. acnes* A1, H1 and H2 EVs (A) Metadata analysis inter-EVs batches and (B) Fluorescence microscopy image of PCi-SEB stained with BODIPY 493/503; negative control (Vehicle), positive control (AA5). All data are presented as mean ± standard deviation (SD) of triplicate measurements (*$p \leq 0.05$, **$p \leq 0.001$ versus non-stimulated controls).